ACADEMIC PRESS

Available online at www.sciencedirect.com
SCIENCE DIRECT®

Journal of Solid State Chemistry 175 (2003) 3–12

JOURNAL OF SOLID STATE CHEMISTRY

http://elsevier.com/locate/jssc

Syntheses, structures, and second-harmonic generating properties in new quaternary tellurites: $A_2TeW_3O_{12}$ (A = K, Rb, or Cs)

Joanna Goodey, Kang Min Ok, Jake Broussard, Cristina Hofmann, Francisco V. Escobedo, and P. Shiv Halasyamani*

Department of Chemistry and the Center for Materials Chemistry, University of Houston, 136 Fleming Building, Houston, TX 77204-5003, USA

Received 2 September 2002; received in revised form 1 January 2003; accepted 8 January 2003

Abstract

The syntheses, structures, and characterization of a new family of quaternary alkali tungsten tellurites, $A_2TeW_3O_{12}$ (A= K, Rb, or Cs), are reported. Crystals of the materials were synthesized by supercritical hydrothermal methods using 1 M AOH (A= K, Rb, or Cs), TeO_2, and WO_3 as reagents. Bulk, polycrystalline phases were synthesized by standard solid-state methods combining stoichiometric amounts of A_2CO_3, TeO_2, and WO_3. Although the three materials are not iso-structural, each exhibits a hexagonal tungsten oxide layer comprised of corner-sharing $W^{6+}O_6$ octahedra. $Te^{4+}O_3$ groups *connect* the WO_6 layers in $K_2TeW_3O_{12}$, whereas the same groups *cap* the WO_6 layers in $Rb_2TeW_3O_{12}$ and $Cs_2TeW_3O_{12}$. This capping results in non-centrosymmetric structures for $Rb_2TeW_3O_{12}$ and $Cs_2TeW_3O_{12}$. Powder second-harmonic generation measurements on $Rb_2TeW_3O_{12}$ and $Cs_2TeW_3O_{12}$ revealed strong SHG efficiencies of 200 and $400 \times SiO_2$, respectively. These values indicate an average non-linear optical susceptibility, $\langle d_{eff} \rangle_{exp}$ of 16 and 23 pm/V for $Rb_2TeW_3O_{12}$ and $Cs_2TeW_3O_{12}$, respectively. Crystallographic information: $K_2TeW_3O_{12}$, monoclinic, space group $P2_1/n$ (No. 14), $a = 7.3224(13)$ Å, $b = 11.669(2)$ Å, $c = 12.708(2)$ Å, $\beta = 90.421(3)^\circ$, $Z = 4$; $Rb_2TeW_3O_{12}$, trigonal, space group $P31c$ (No. 159), $a = b = 7.2980(2)$ Å, $c = 12.0640(2)$ Å, $Z = 2$.

Keywords: Synthesis; Oxides; Non-linear optics; Non-centrosymmetric tellurites

1. Introduction

The demand for new and superior performing non-linear optical (NLO), i.e., second-harmonic generating (SHG) materials [1–5] for use in optical devices remains strong [6]. Despite this demand, the discovery of enhanced NLO materials is hindered by the lack of understanding of the structure–property relationships associated with the phenomenon. One necessary criterion for SHG, crystallographic non-centrosymmetry (NCS), has been established [7]. In addition to being NCS, viable SHG materials should be chemically stable, transparent in the relevant wavelengths, and able to withstand laser irradiation. With inorganic materials, macroscopic NCS is often a consequence of the acentric coordination of certain metal cations. This local acentricity is a necessary, but not sufficient condition for generating crystallographic NCS. In other words, the material may crystallize with the acentric units aligned in an anti-parallel manner, resulting in crystallographic centrosymmetry. In a review of NCS oxides [3], we determined the influence of a second-order Jahn–Teller (SOJT) distortion [8–14] on the NCS structure. A strategy that we have employed to create NCS materials involves synthesizing compounds that contain cations susceptible to SOJT distortions, i.e., d^0 transition metals (Ti^{4+}, Nb^{5+}, or W^{6+}) and cations with non-bonded electron pairs (Se^{4+}, Te^{4+}, or Sb^{3+}) [15–20].

Other than crystallographic NCS, one common structural feature of highly efficient SHG materials, i.e., a SHG response $>400 \times SiO_2$, is the "constructive addition" of the individual bond hyperpolarizabilities, β(M–O). It is this "constructive addition" of bond hyperpolarizabilities that is thought to be responsible for the large SHG responses found in $KTiOPO_4$ (KTP), $LiNbO_3$, and $BaTiO_3$ [21–24]. Our particular investigation into understanding the structural origin of the second-order NLO effect focuses on the synthesis of new alkali tungsten tellurites. It is anticipated that the

*Corresponding author. Fax: +1-713-743-3278.
E-mail address: psh@uh.edu (P.S. Halasyamani).

0022-4596/03/$ - see front matter © 2003 Elsevier Inc. All rights reserved.
doi:10.1016/S0022-4596(03)00079-3

coupling of the SOJT distortion of a d^0 metal, W^{6+}, with that of Te^{4+} will promote the formation of a material with a strong SHG response.

To date, a number of A^+–M^{6+}–Te^{4+}–O (where A = Na, K, Rb, or Cs; M = Mo or W) compounds have been reported [20,25–28]. Crystallizing with zero-, one-, two- and three-dimensional networks these quaternary tellurites are structurally diverse. Two noteworthy non-centrosymmetric compounds, $Na_2TeW_2O_9$ [20] and $Cs_2Mo_3TeO_{12}$ [26], both produce large SHG responses ($>400\times SiO_2$). Here we present the synthesis, structure, and characterization of the new alkali tungsten tellurites, $K_2TeW_3O_{12}$, $Rb_2TeW_3O_{12}$, and $Cs_2TeW_3O_{12}$. Although each of these compounds crystallizes in a different space group, $P2_1/n$, $P31c$, and $P6_3$ for $K_2TeW_3O_{12}$, $Rb_2TeW_3O_{12}$, and $Cs_2TeW_3O_{12}$, respectively, all contain the corner-sharing hexagonal tungsten oxide layer illustrated in Scheme 1. Similar to that found in hexagonal WO_3 [29], the $[M_3O_{12}]^{6-}$ network, also exists in quaternary selenites [30–33] and $Cs_2Mo_3TeO_{12}$ [26]. In centrosymmetric $K_2TeW_3O_{12}$ the TeO_3 groups *connect* adjacent layers, whereas in non-centrosymmetric $Cs_2TeW_3O_{12}$ and $Rb_2TeW_3O_{12}$ three-coordinate pyramidal TeO_3 groups *cap* the tungsten oxide layers. The effect of cation size on the structure, more specifically on the symmetry and the accompanying SHG response is illustrated by these three new structurally related tellurites.

2. Experimental

2.1. Reagents

TeO_2 (Aldrich, 99%), WO_3 (Aldrich, 99%), Cs_2CO_3 (Alfa Aesar, 99.9%), Rb_2CO_3 (Aldrich, 99.8%), K_2CO_3 (Alfa Aesar, 99.0%), CsOH (Aldrich, 99.9%), RbOH (Aldrich, 99.9%), and KOH (EM Science, 90%) were used as received.

2.2. Syntheses

Single crystals of $A_2TeW_3O_{12}$ (A = K, Rb, or Cs) were initially prepared hydrothermally from a solution of AOH (A = K, Rb, or Cs), WO_3, and TeO_2. The oxides, WO_3 and TeO_2, were combined with 1 M AOH in separate gold tubes. For $K_2TeW_3O_{12}$ 0.060 g (3.75×10^{-4} mol) of TeO_2 and 0.058 g (2.50×10^{-4} mol) of WO_3 were combined with 0.208 mL of 1 M (2.08×10^{-4} mol) KOH. For $Rb_2TeW_3O_{12}$ 0.0097 g (6.05×10^{-5} mol) of TeO_2 and 0.056 g (2.43×10^{-4} mol) of WO_3 were combined with 0.304 mL of 1 M (3.04×10^{-4} mol) RbOH. For $Cs_2TeW_3O_{12}$ 0.011 g (6.60×10^{-5} mol) of TeO_2 and 0.046 g (1.98×10^{-4} mol) of WO_3 were combined with 0.395 mL of 1 M (3.95×10^{-4} mol) CsOH. The gold tubes (i.d. = 4.6 mm, o.d. = 4.9 mm, and lengths = 40.0–62.0 mm) were welded, closed and placed into a LECO autoclave. The autoclave was filled with 18 mL (60% fill) of H_2O, sealed, and heated to 470°C. At 470°C an autogenous pressure of 6500 psi (442 atm) was observed. After 48 h at 470°C the autoclave was cooled slowly (6°C h^{-1}) to room temperature. The gold tubes were retrieved from the autoclave and opened. Crystals of $K_2TeW_3O_{12}$ (colorless square columns), $Rb_2TeW_3O_{12}$ (yellow hexagonal plates), and $Cs_2TeW_3O_{12}$ (pale-yellow hexagonal plates) were retrieved by filtration. The yields of the recovered products based on TeO_2 ranged from 60% to 70%. Colorless needles of TeO_2 were also present.

Bulk, polycrystalline samples of $K_2TeW_3O_{12}$, $Rb_2TeW_3O_{12}$, and $Cs_2TeW_3O_{12}$ were obtained by standard

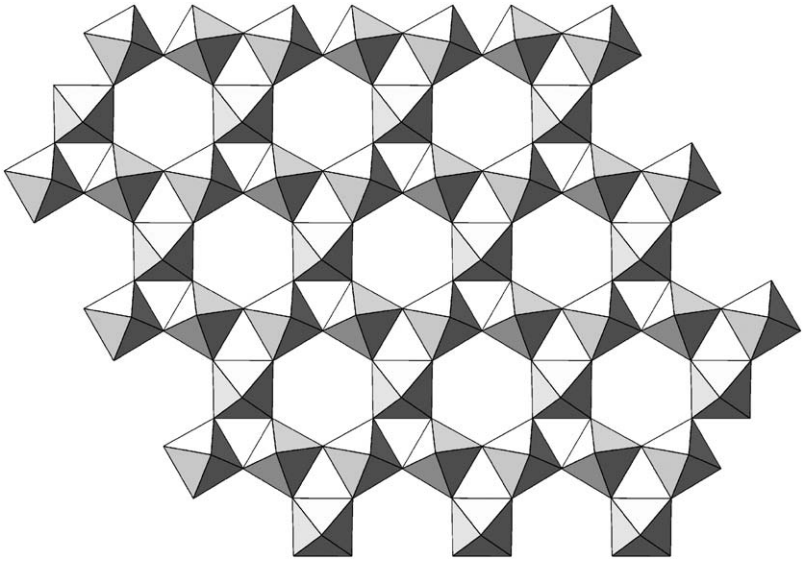

Scheme 1.

solid-state methods. Stoichiometric amounts of A_2CO_3 (A = K, Rb, or Cs), TeO_2, and WO_3 were ground and pressed into pellets that were heated in air to 450°C for 10 h and then to 600°C for 3d with three intermittent re-grindings.

2.3. Single-crystal X-ray diffraction

For $K_2TeW_3O_{12}$ a colorless rod ($0.1 \times 0.16 \times 0.20\,mm^3$), for $Rb_2TeW_3O_{12}$ a colorless plate ($0.04 \times 0.08 \times 0.14\,mm^3$), and for $Cs_2TeW_3O_{12}$ a colorless plate ($0.02 \times 0.1 \times 0.1\,mm^3$) was used for single-crystal data analyses. Data were collected using an Enraf Nonius FR 590 Kappa CCD diffractometer with graphite monochromated Mo$K\alpha$ radiation (λ = 0.71073 Å). Crystals were mounted on a glass fiber using n-paratone oil and cooled in situ using an Oxford Cryostream 600 Series to 150 K for data collection. Frames were collected, indexed, and processed using Denzo SMN and the files scaled together using HKL GUI within Denzo SMN [34]. The data were solved and refined using SHELXS-97 and SHELXL-97, respectively [35,36]. All calculations were performed using the WinGX-98 crystallographic software package [37]. Relevant crystallographic data are listed in Table 1, atomic coordinates are given in Tables 2 and 3, and selected bond distances are given in Table 4. Although crystals of $Cs_2TeW_3O_{12}$ were grown, data were collected, and a solution was obtained, satisfactory refinements did not occur. However, based on the single-crystal data solution as well as powder X-ray diffraction data we were able to confirm that $Cs_2TeW_3O_{12}$ is iso-structural to $Cs_2TeMo_3O_{12}$ [26]. Table 5 gives the refined unit cell parameters, space group, h,k,l, d(obs), d(calc), I(obs), and I(calc) for $Cs_2TeW_3O_{12}$. The experimental and calculated powder X-ray

Table 2
Atomic coordinates for $K_2TeW_3O_{12}$

Atom	x	y	z	$U_{(eq)}$(Å^2)
K1	0.2515(9)	−0.5474(6)	−0.0804(5)	0.0268(14)
K2	0.2572(10)	0.0713(7)	−0.1113(6)	0.0331(16)
W1	0.22662(13)	−0.20272(8)	−0.92105(7)	0.0083(2)
W2	0.01970(13)	−0.25669(8)	−0.18111(7)	0.0087(2)
W3	0.50923(13)	−0.24629(8)	−0.15862(7)	0.0082(2)
Te1	0.2506(2)	−0.49534(13)	−0.80291(12)	0.0097(3)
O1	0.438(2)	−0.5796(15)	−0.8680(14)	0.012(3)[a]
O2	0.062(3)	−0.5777(17)	−0.8714(15)	0.019(4)
O3	0.255(2)	−0.3801(16)	−0.9030(14)	0.014(4)
O4	0.069(2)	−0.2007(16)	−0.8133(14)	0.014(4)
O5	0.443(3)	−0.2297(18)	−0.0242(16)	0.022(4)
O6	0.060(3)	−0.2375(17)	−0.0263(16)	0.022(4)
O7	0.245(3)	−0.0564(18)	−0.9448(16)	0.022(4)
O8	0.058(3)	−0.1135(17)	−0.2100(15)	0.019(4)
O9	−0.069(2)	−0.3050(15)	−0.3112(13)	0.011(3)
O10	0.256(2)	−0.3127(16)	−0.1966(14)	0.015(4)
O11	0.445(3)	−0.1128(16)	−0.2124(14)	0.015(4)
O12	0.755(2)	−0.2171(14)	−0.1434(13)	0.007(3)

$U_{(eq)}$ is defined as one-third of the trace of the orthogonalized U_{ij} tensor.
[a] All oxygen atoms were refined isotropically.

Table 1
Crystallographic data for $K_2TeW_3O_{12}$ and $Rb_2TeW_3O_{12}$

	$K_2TeW_3O_{12}$	$Rb_2TeW_3O_{12}$
Formula weight	949.35	1042.09
Temperature (K)	150.0(1)	150.0(1)
Wavelength (Å)	0.71073	0.71073
Crystal system, space group	Monoclinic, $P2_1/n$ (No. 14)	Trigonal, $P31c$ (No. 159)
Unit-cell dimensions	a = 7.3224(13) Å	a = 7.2980(2) Å
	b = 11.669(2) Å	b = 7.2980(2) Å
	c = 12.708(2) Å	c = 12.0640(2) Å
	β = 90.421(3)°	$\alpha = \beta = 90°$, $\gamma = 120°$
Volume (Å^3), Z	1085.8(3), 4	556.5(3), 2
$\rho_{(calc)}$, $\rho_{(exp)}$ (g/cm^3)	5.807, 5.920(1)[a]	6.219, 6.280(1)[a]
Absorption coeff. (mm^{-1})	35.162	42.248
Crystal size (mm)	0.1 × 0.16 × 0.2	0.04 × 0.08 × 0.14
Reflections collected/unique	6640/2451 [R(int) = 0.0546]	2629/718 [R(int) = 0.0578]
Absorption correction	Analytical	Analytical
Max. and min. transmission	0.193 and 0.150	0.638 and 0.033
Refinement method	Full-matrix least squares on F^2	Full-matrix least squares on F^2
Goodness-of-fit on F^2	1.288	1.249
Final $R^{b,c}$ indices [$I > 2\sigma(I)$]	R = 0.0621, R_w = 0.1472	R = 0.0611, R_w = 0.1635
R indices (all data)	R = 0.0656, R_w = 0.1486	R = 0.0614, R_w = 0.1640
Extinction coefficient	0.00000(5)	0.0033(9)
Absolute structure parameter	N/A	0.58(7)

[a] Density measured by gas pycnometry [38].
[b] $R = \sum||F_o| - |F_c||/\sum|F_o|$.
[c] $R_w = [\sum w(F_o^2 - F_c^2)^2/\sum w(F_o^2)^2]^{1/2}$.

Table 3
Atomic coordinates for $Rb_2TeW_3O_{12}$

Atom	x	y	z	$U_{(eq)}$ (Å^2)
Rb1	0.3333	−0.3333	−0.1459(14)	0.052(4)
Rb2	0.3333	−0.3333	0.4857(15)	0.054(4)
Te1	0.0000	0.0000	−0.0772(4)	0.0095(9)
W1	0.1952(2)	−0.1441(2)	0.17289(17)	0.0068(6)
O1	0.464(5)	−0.075(6)	0.139(3)	0.032(8)[a]
O2	0.128(6)	−0.124(6)	0.001(4)	0.041(9)
O3	0.255(4)	0.121(4)	0.187(2)	0.004(4)
O4	0.193(6)	−0.185(5)	0.313(3)	0.027(7)

$U_{(eq)}$ is defined as one-third of the trace of the orthogonalized U_{ij} tensor.
[a] All oxygen atoms were refined isotropically.

Table 4
Selected bond distances (Å) for $K_2TeW_3O_{12}$ and $Rb_2TeW_3O_{12}$

$K_2TeW_3O_{12}$		$Rb_2TeW_3O_{12}$	
Te–O1	1.884(18)	Te1–O2	1.85(5)
Te–O2	1.89(2)	Te1–O2	1.85(5)
Te–O3	1.851(18)	Te1–O2	1.85(5)
W1–O3	2.093(18)	W1–O1	1.81(3)
W1–O4	1.799(18)	W1–O1	2.06(4)
W1–O5	2.09(2)	W1–O2	2.16(4)
W1–O6	1.85(2)	W1–O3	2.12(2)
W1–O7	1.74(2)	W1–O3	1.77(2)
W1–O9	2.039(17)	W1–O4	1.72(4)
W2–O2	2.13(2)		
W2–O6	2.00(2)		
W2–O8	1.73(2)		
W2–O9	1.860(17)		
W2–O10	1.861(18)		
W2–O12	2.054(16)		
W3–O1	2.095(17)		
W3–O4	2.109(18)		
W3–O5	1.79(2)		
W3–O10	2.064(18)		
W3–O11	1.762(18)		
W3–O12	1.839(16)		

diffraction patterns for $K_2TeW_3O_{12}$ and $Rb_2TeW_3O_{12}$ have been deposited.

2.4. Infrared spectroscopy

Infrared spectra were recorded on a Matteson FTIR 5000 spectrometer in the 400–4000 cm^{-1} range, with the sample pressed between two KBr pellets.

Thermogravimetric analysis: Thermogravimetric analyses were carried out on a TGA 2950 thermogravimetric analyzer (TA instruments). The sample was contained within a platinum crucible and heated in air at a rate of 5°C/min to 950°C.

Table 5
Powder X-ray diffraction data for $Cs_2TeW_3O_{12}$ [refined unit cell[a] $a = b = 7.327(2)$ Å, $c = 12.397(2)$ Å, $\alpha = \beta = 90°$, $\gamma = 120°$; space group $P6_3$ (No. 173)]

h	k	l	d_{obs}	d_{calc}	I_{obs}	I_{calc}[a]
0	1	0	6.349	6.343	11	11
0	0	2	6.202	6.199	27	28
0	1	1	5.651	5.647	12	11
0	1	2	4.432	4.433	1	1
1	1	0	3.662	3.663	8	11
1	1	1	3.508	3.513	3	3
0	1	3	3.462	3.463	57	58
0	2	0	3.174	3.172	16	22
1	1	2	3.153	3.154	87	95
0	0	4	3.099	3.099	25	29
0	2	1	3.073	3.073	100	100
0	2	2	2.823	2.824	21	21
0	1	4	2.784	2.785	14	13
0	2	3	2.516	2.516	4	3
1	2	0	2.399	2.398	2	2
1	1	4	2.366	2.366	2	2
0	1	5	2.309	2.309	2	1
0	2	4	2.216	2.217	1	1
0	3	0	2.114	2.114	1	1
2	1	3	2.074	2.074	11	11
0	0	6	2.066	2.066	9	8
0	3	2	2.001	2.001	17	15
0	1	6	1.964	1.965	2	2
0	2	5	1.953	1.953	26	23
2	2	0	1.831	1.832	27	26
1	1	6	1.801	1.800	2	2
2	2	2	1.757	1.756	3	3
3	1	1	1.743	1.742	2	2
0	2	6	1.731	1.731	13	14
0	1	7	1.706	1.706	1	2
1	3	2	1.693	1.693	1	1
1	3	3	1.619	1.619	3	5
0	4	0	1.586	1.586	1	2
2	2	4	1.577	1.577	11	12
0	4	1	1.573	1.573	9	9
1	2	6	1.564	1.565	1	1
0	2	7	1.546	1.546	7	7
0	4	2	1.536	1.536	3	4
1	3	4	1.530	1.530	4	5
0	1	8	1.506	1.505	2	3

Calculated using the atomic coordinates for $Cs_2Mo_3TeO_{12}$ [26] but substituting tungsten for molybdenum.
[a] The unit cell was determined by using the program ERACEL [46].

2.5. Density

Powder density measurements were performed on polycrystalline $K_2TeW_3O_{12}$ and $Rb_2TeW_3O_{12}$ using a gas pycnometry [38].

2.6. Second-order non-linear optical measurements

Powder SHG measurements on $Rb_2TeW_3O_{12}$ and $Cs_2TeW_3O_{12}$ were performed on a modified Kurtz-NLO [39] system using 1064 nm radiation. A detailed description of the equipment and the methodology used has

been published [16,18]. No index matching fluid was used in any of the experiments. Powders with particle size 45–63 μm were used for comparing SHG intensities.

3. Results and discussion

As $Cs_2TeW_3O_{12}$ is iso-structural to $Cs_2TeMo_3O_{12}$ [26], only a detailed structural description of $K_2TeW_3O_{12}$ and $Rb_2TeW_3O_{12}$ will be given. $K_2TeW_3O_{12}$ has a three-dimensional crystal structure consisting of layers of corner-shared WO_6 octahedra connected by asymmetric TeO_3 groups (see Figs. 1 and 2). The TeO_3 groups serve as an *inter-layer* linker. Each W^{6+} cation is connected to six oxygen atoms in an octahedral arrangement. Five of the six oxygen atoms either link to another W^{6+} cation or a Te^{4+} cation. The remaining oxygen atom is single bonded only to W^{6+} and points toward the K^+ cation. The WO_6 octahedra form a hexagonal motif (see Scheme 1) that is common to all three reported compounds. The W–O and Te–O bond distances range from 1.73(2) to 2.109(18) Å and

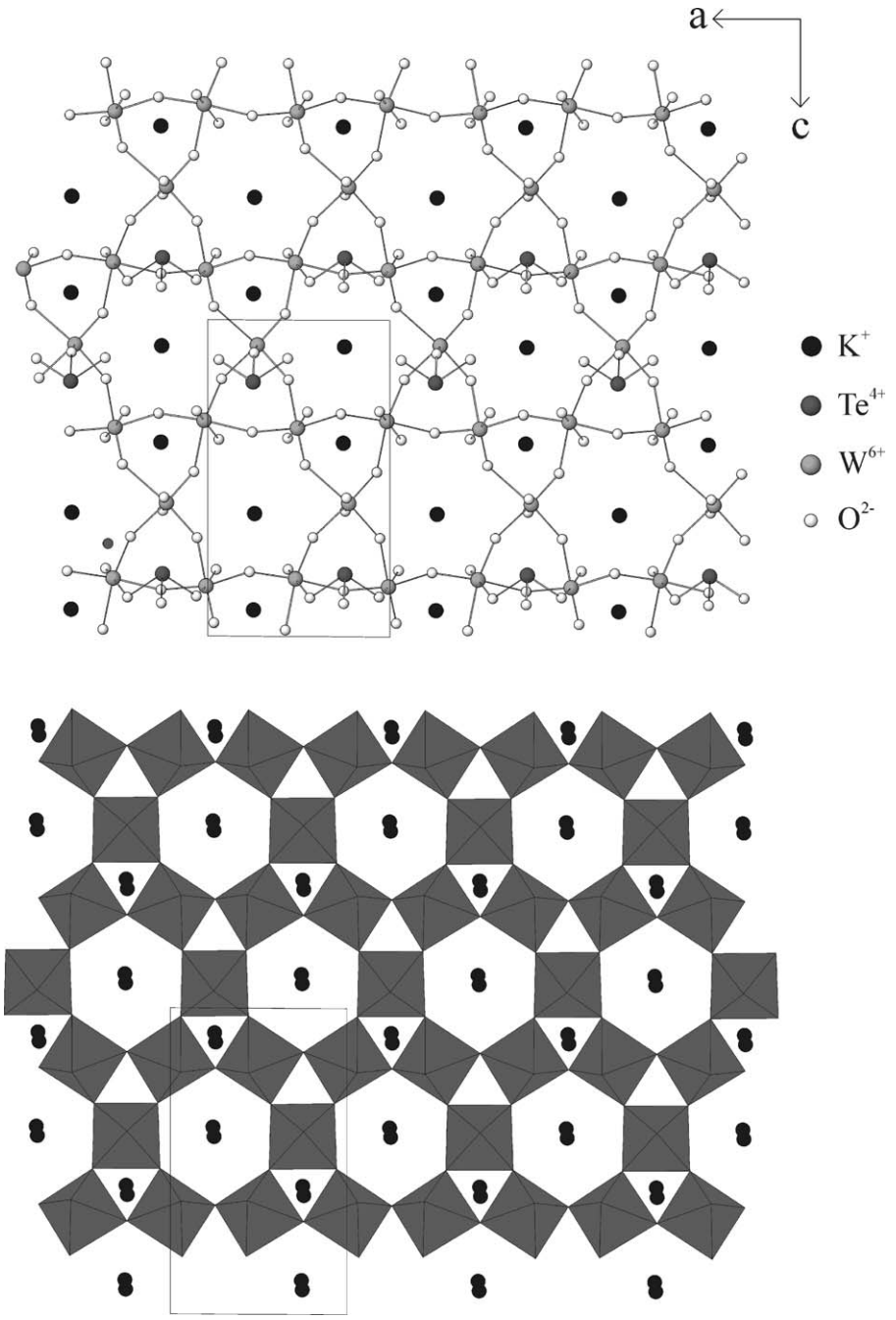

Fig. 1. Ball-and-stick (top) and polyhedral (bottom) representation of $K_2TeW_3O_{12}$ in the *ac*-plane.

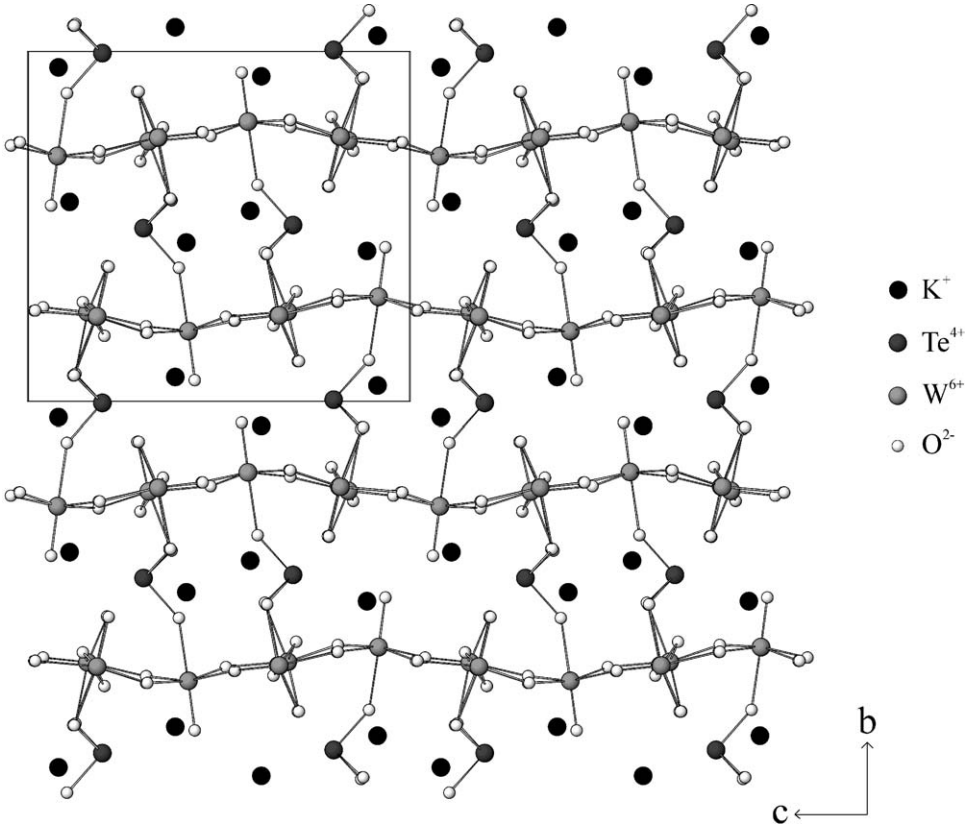

Fig. 2. Ball-and-stick representation of $K_2TeW_3O_{12}$ in the *bc*-plane.

1.851(18) to 1.89(2) Å, respectively. The K^+ cations are in six- and seven-fold coordination environments with K–O contacts ranging from 2.57(2) to 3.32(2) Å. In terms of connectivity the structure can be written as $\{[TeO_{3/2}]^+[WO_{5/2}O_{1/1}]_3^-\}^{2-}$, with charge balance maintained by the two K^+ cations. Bond valence [40,41] calculations resulted in values ranging from 6.05 to 6.16 for W^{6+} and 3.96 for Te^{4+}.

$Rb_2TeW_3O_{12}$ has a layered crystal structure, consisting of corner-shared WO_6 octahedra capped by asymmetric TeO_3 groups (see Figs. 3 and 4). In $Rb_2TeW_3O_{12}$ and $Cs_2TeW_3O_{12}$, the TeO_3 groups serve as *intra-layer* linkers. The W^{6+} cation is bonded to six oxygen atoms resulting in an octahedral arrangement. As with $K_2TeW_3O_{12}$, five of the six oxygen atoms are linked to another W^{6+} cation or a Te^{4+} cation. The remaining oxygen atom is singly bonded to W^{6+} and points toward the Rb^+ cations. The W–O bond distances range from 1.72(4) to 2.16(4) Å with a unique Te–O bond distance of 1.85(5) Å. The Rb^+ cations are in six- and nine-fold coordination environments with Rb–O contacts ranging from 2.68(4) to 3.47(4) Å. In connectivity terms the structure can be written as $\{[TeO_{3/2}]^+[WO_{5/2}O_{1/1}]_3^-\}^{2-}$, with charge balance maintained by the two Rb^+ cations. Bond valence [40,41] calculations resulted in values of 6.30 and 4.23 for W^{6+} and Te^{4+}, respectively.

As previously stated, although $K_2TeW_3O_{12}$, $Rb_2TeW_3O_{12}$, and $Cs_2TeW_3O_{12}$ are stoichiometrically "equivalent", the materials are not iso-structural. However, all three phases share a common structural motif, a two-dimensional hexagonal WO_6 network (see Scheme 1). This planar network of corner-shared WO_6 octahedra is similar to those found in three-dimensional WO_3 [29] and alkali-metal tungsten bronzes. Each WO_6 octahedron is corner shared, through oxygen, with four other WO_6 octahedra forming a hexagonal network of six- and three-member rings. The alkali cations occupy all of the cavities formed by the six-member rings and half of the cavities formed by the three-member rings. Interestingly, the size of the alkali cation influences the nature of the TeO_3-group bonding, i.e., connecting compared to capping the WO_6 layers. Furthermore, this TeO_3-group bonding determines the symmetry, centrosymmetric or non-centrosymmetric, of the material.

Scheme 1 depicts the common WO_6 layer observed in all these compounds. In all three materials this layer is pseudo-centrosymmetric, indicating that the acentricity observed in $Rb_2TeW_3O_{12}$ and $Cs_2TeW_3O_{12}$ is wholly attributable to the asymmetric TeO_3 group. But the question remains, why is $K_2TeW_3O_{12}$ centrosymmetric? Structurally, the centricity in $K_2TeW_3O_{12}$ is attributable to not only the arrangement of the WO_6 octahedra, but also the TeO_3 groups. In all three materials the

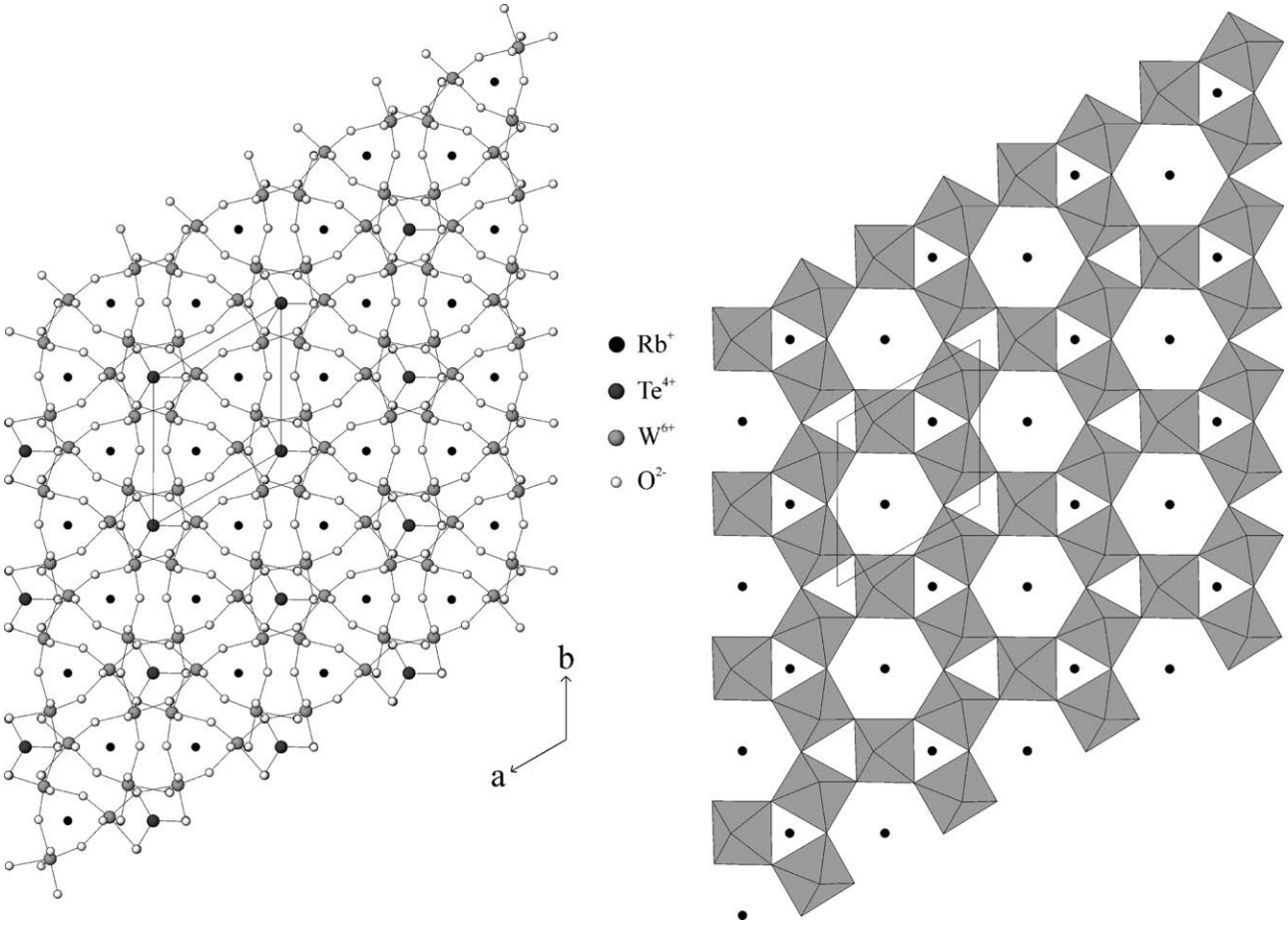

Fig. 3. Ball-and-stick (left) and polyhedral (right) representation of $Rb_2TeW_3O_{12}$ in the *ab*-plane.

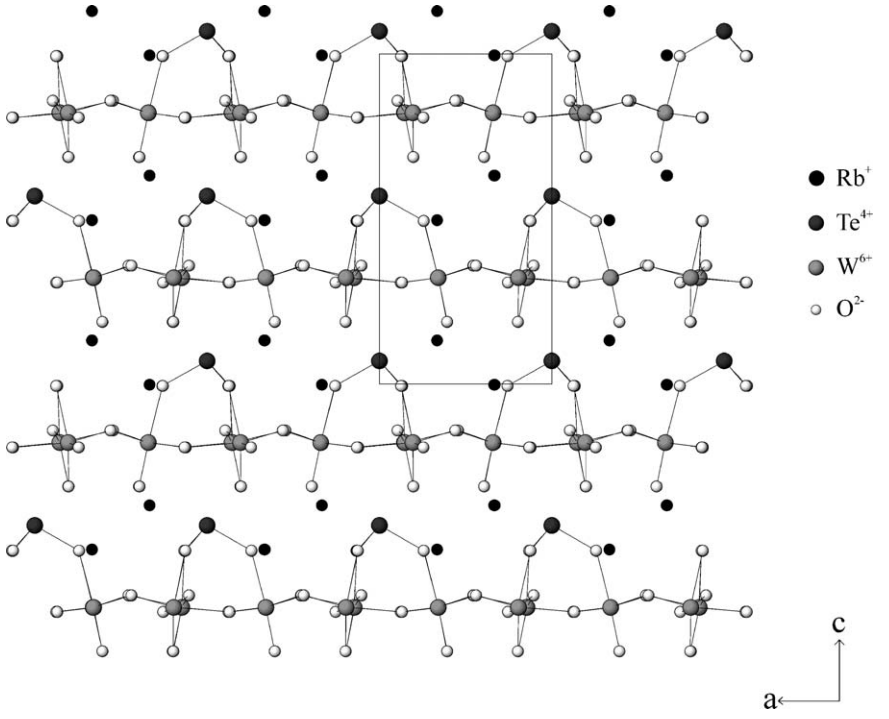

Fig. 4. Ball-and-stick representation of $Rb_2TeW_3O_{12}$ in the *ac*-plane.

alkali-cations reside between the WO_6 layers. Taken from Shannon [42], the average radii for K^+, Rb^+, and Cs^+ are 1.42, 1.58, and 1.78 Å, respectively. The increasing size of the alkali-metal pushes the WO_6 layers further apart. In $K_2TeW_3O_{12}$ the closest inter-layer O–O contact is 2.65 Å, whereas in $Rb_2TeW_3O_{12}$ and $Cs_2TeW_3O_{12}$ the analogous distances are 3.18 and 3.25 Å, respectively. The smaller inter-layer spacing in $K_2TeW_3O_{12}$ allows the Te^{4+} to connect the layers, bonding to oxygen atoms in adjacent layers. Since the TeO_3 groups connect the layers, the lone-pair–lone-pair repulsions are minimized by pointing in opposite directions [001] and [00$\bar{1}$], i.e., a centrosymmetric arrangement. Thus the net symmetry of $K_2TeW_3O_{12}$ is centrosymmetric. Conversely, the larger inter-layer spacing in $Rb_2TeW_3O_{12}$ and $Cs_2TeW_3O_{12}$ forces the Te^{4+} to bond to three oxygen atoms within one layer, as the nearest Te–O contact on an adjacent layer is at a distance of 2.84 Å. Thus in both $Rb_2TeW_3O_{12}$ and $Cs_2TeW_3O_{12}$ the TeO_3 groups cap the WO_6 layers, with the lone-pair on Te^{4+} pointing along the [001] direction. In order to minimize lone-pair–lone-pair interactions, adjacent layers are similarly capped. Thus $Rb_2TeW_3O_{12}$ and $Cs_2TeW_3O_{12}$ have non-centrosymmetric structures. Fig. 5 depicts the inter-layer O–O distances in all three materials.

3.1. Infrared spectroscopy

The infrared spectra of all $A_2TeW_3O_{12}$ (A = K, Cs, Rb) compounds reveal several W–O, Te–O and W–O–Te vibrations found in the region between 600 and 950 cm^{-1}. The stretches between 770 and 950 cm^{-1} can be attributed to the W–O vibrations [25]. The stretches between 600 and 950 cm^{-1} represent a combination of the W–O, Te–O, and W–O–Te vibrations [43–45].

3.2. Thermogravimetric analysis

The thermal behavior of the $A_2TeW_3O_{12}$ (A = K, Cs, Rb) compounds was investigated using thermogravimetric

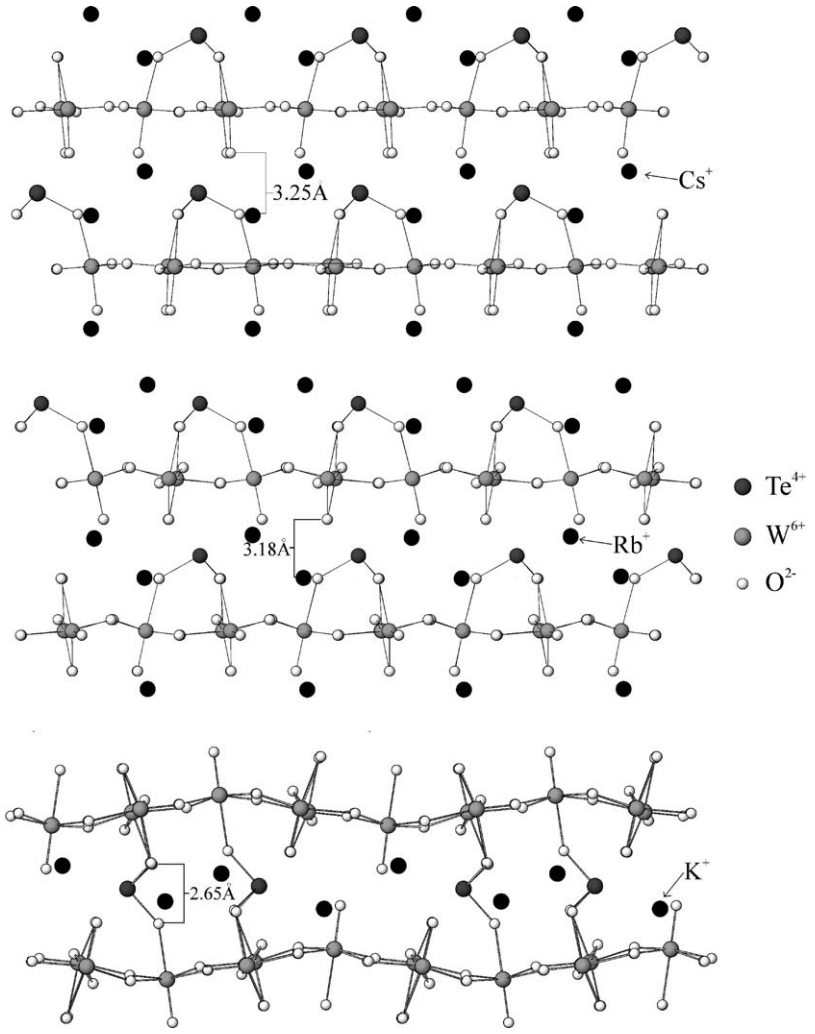

Fig. 5. Ball-and-stick representation of the 'layers' in $K_2TeW_3O_{12}$ (bottom), $Rb_2TeW_3O_{12}$ (middle), and $Cs_2TeW_3O_{12}$ (top) indicating the closest inter-layer O–O distance.

analysis. In each case a single step decomposition occurs indicating volatilization above 700°C for $K_2TeW_3O_{12}$, 720°C for $Rb_2TeW_3O_{12}$, and 730°C for $Cs_2TeW_3O_{12}$.

3.3. Second-order non-linear optical measurements

SHG measurements and sieved $Rb_2TeW_3O_{12}$ and $Cs_2TeW_3O_{12}$ indicate the materials are phase-matchable (Type 1) (see Fig. 6) with efficiencies of approximately 200 and $400 \times SiO_2$, respectively. These efficiencies compare reasonably well with respect to $BaTiO_3$ ($400 \times SiO_2$) and $LiNbO_3$ ($600 \times SiO_2$). As we have previously published [20], once the phase-matching behavior has been determined and SHG efficiency has been measured, the experimental average NLO susceptibility, $\langle d_{\text{eff}} \rangle_{\text{exp}}$, can be estimated. For phase-matchable materials

$$\langle d_{\text{eff}} \rangle_{\text{exp}} = \left[7.98 \times 10^2 \left(\frac{I^{2\omega}_{A_2TeW_3O_{12}}}{I^{2\omega}_{LiNbO_3}} \right) \right]^{1/2},$$

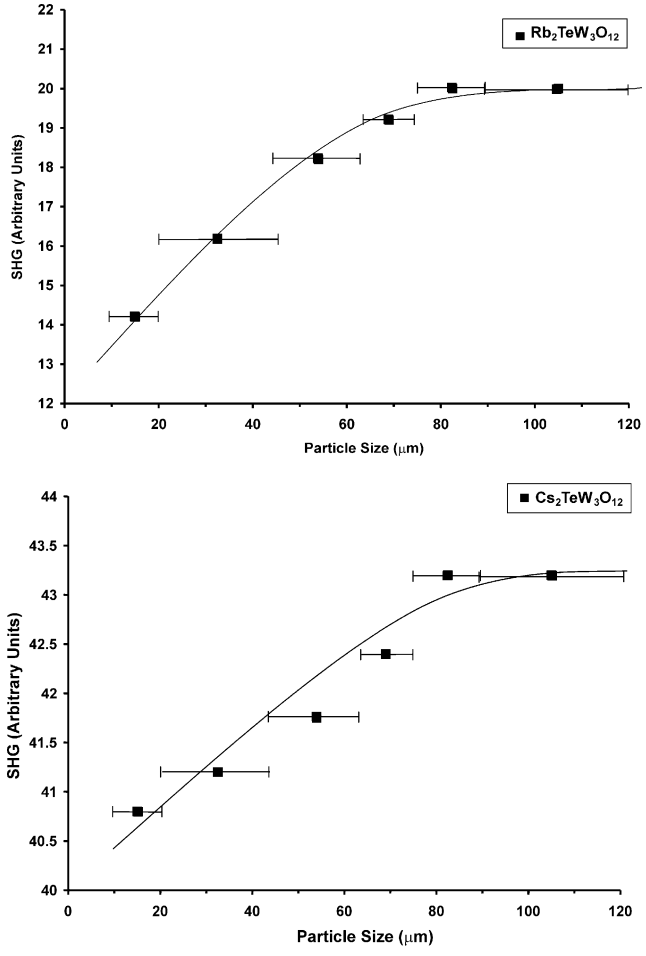

Fig. 6. Phase-matching curves for $Rb_2TeW_3O_{12}$ and $Cs_2TeW_3O_{12}$. Note the lines are drawn to guide the eye and are not a fit to the data.

where $I^{2\omega}_{LiNbO_3}$ is the SHG efficiency of $LiNbO_3$ compared to SiO_2. Since $I^{2\omega}_{LiNbO_3} = 600$, $I^{2\omega}_{Rb_2TeW_3O_{12}} = 200$, and $I^{2\omega}_{Cs_2TeW_3O_{12}} = 400$;

$$\langle d_{\text{eff}}^{Rb_2TeW_3O_{12}} \rangle_{\text{exp}} = 16 \text{ pm/V}$$

and

$$\langle d_{\text{eff}}^{Cs_2TeW_3O_{12}} \rangle_{\text{exp}} = 23 \text{ pm/V}.$$

One of our goals in investigating SHG materials is to determine the structural origin of the NLO response. As previously stated, the hexagonal WO_6 layer in $Rb_2TeW_3O_{12}$ and $Cs_2TeW_3O_{12}$ is centrosymmetric. Thus the observed SHG response can be wholly attributed to the polarization from the TeO_3 group. We have estimated a bond hyperpolarizability, β, for a Te–O bond to be 130×10^{-40} m^4/V [20]. The structural model allows us to use β(Te–O) and calculate $\langle d_{\text{eff}} \rangle$ for $Rb_2TeW_3O_{12}$ and $Cs_2TeW_3O_{12}$. We calculate $\langle d_{\text{eff}}^{Rb_2TeW_3O_{12}} \rangle_{\text{calc}} = 23$ pm/V and $\langle d_{\text{eff}}^{Cs_2TeW_3O_{12}} \rangle_{\text{calc}} = 29$ pm/V that are in reasonable agreement with our experimental values of $\langle d_{\text{eff}}^{Rb_2TeW_3O_{12}} \rangle_{\text{exp}} = 16$ pm/V and $\langle d_{\text{eff}}^{Cs_2TeW_3O_{12}} \rangle_{\text{exp}} = 23$ pm/V.

4. Summary

We have synthesized and characterized three new tellurites in the $A_2TeW_3O_{12}$ family ($A = K^+$, Rb^+, or Cs^+). The materials consist of WO_6 octahedra and TeO_3 groups that are linked to form either three-dimensional ($K_2TeW_3O_{12}$) or layered ($Rb_2TeW_3O_{12}$ and $Cs_2TeW_3O_{12}$) topologies. Crystallographic data indicate $K_2TeW_3O_{12}$ is centrosymmetric, whereas $Rb_2TeW_3O_{12}$ and $Cs_2TeW_3O_{12}$ are non-centrosymmetric. The respective symmetries of the materials can be understood by examining the size of the A-cation. Powder SHG measurements on $Rb_2TeW_3O_{12}$ and $Cs_2TeW_3O_{12}$ indicate both materials are phase-matchable (Type 1) with intensities of 200 and $400 \times SiO_2$, respectively. These efficiencies correspond to $\langle d_{\text{eff}} \rangle$ of 16 and 23 pm/V for $Rb_2TeW_3O_{12}$ and $Cs_2TeW_3O_{12}$, respectively. We are in the process of synthesizing other NCS materials and will be reporting on them shortly.

Acknowledgments

P.S.H. thanks the Inorganic Chemistry Laboratory and Chemical Crystallography both at the University of Oxford for assistance during his recent visit. We thank the Robert A. Welch Foundation for support. This work was also supported by the NSF-Career Program through DMR-0092054 and an acknowledgment is made to the donors of The Petroleum Research Fund, administered by the American Chemical Society, for

partial support of this research. P.S.H. is a Beckman Young Investigator.

Supporting information available

Powder X-ray diffraction patterns (calculated and experimental) are available (PDF). A file of X-ray crystallographic data is also available (CIF).

References

[1] S.R. Marder, J.E. Sohn, G.D. Stucky, Materials for Non-linear Optics: Chemical Perspectives, ACS, Washington, DC, 1991.
[2] C. Chen, G. Liu, Ann. Rev. Mater. Sci. 16 (1986) 203.
[3] P.S. Halasyamani, K.R. Poeppelmeier, Chem. Mater. 10 (1998) 2753.
[4] P. Becker, Adv. Mater. 10 (1998) 979.
[5] D.A. Keszler, Curr. Opin. Solid State Mater. Sci. 4 (1999) 155.
[6] O. Auciello, J.F. Scott, R. Ramesh, Phys. Today 40 (1998) 22.
[7] J.F. Nye, Physical Properties of Crystals, Oxford University Press, Oxford, 1957.
[8] U. Opik, M.H.L. Pryce, Proc. R. Soc. (London) A 238 (1957) 425.
[9] R.F.W. Bader, Mol. Phys. 3 (1960) 137.
[10] R.F.W. Bader, Can. J. Chem. 40 (1962) 1164.
[11] R.G. Pearson, J. Am. Chem. Soc. 91 (1969) 4947.
[12] R.G. Pearson, J. Mol. Struct. (Theochem) 103 (1983) 25.
[13] R.A. Wheeler, M.-H. Whangbo, T. Hughbanks, R. Hoffmann, J.K. Burdett, T.A. Albright, J. Am. Chem. Soc. 108 (1986) 2222.
[14] M. Kunz, I.D. Brown, J. Solid State Chem. 115 (1995) 395.
[15] Y. Porter, N.S.P. Bhuvanesh, P.S. Halasyamani, Inorg. Chem. 40 (2001) 1172.
[16] Y. Porter, K.M. Ok, N.S.P. Bhuvanesh, P.S. Halasyamani, Chem. Mater. 13 (2001) 1910.
[17] K.M. Ok, N.S.P. Bhuvanesh, P.S. Halasyamani, Inorg. Chem. 40 (2001) 1978.
[18] K.M. Ok, N.S.P. Bhuvanesh, P.S. Halasyamani, J. Solid State Chem. 161 (2001) 57.
[19] Y. Porter, P.S. Halasyamani, Inorg. Chem., 2002, submitted for publication.
[20] J. Goodey, J. Broussard, P.S. Halasyamani, Chem. Mater. 14 (2002) 3174.
[21] C.R. Jeggo, G.D. Boyd, J. Appl. Phys. 41 (1970) 2741.
[22] M. DiDomenico, S.H. Wemple, J. Appl. Phys. 40 (1969) 720.
[23] B.F. Levine, IEEE J. Quantum Electron. QE-9 (1973) 946.
[24] J.G. Bergman, G.R. Crane, J. Solid State Chem. 12 (1975) 172.
[25] V. Balraj, K. Vidyasagar, Inorg. Chem. 38 (1999) 5809.
[26] B. Vidyavathy, K. Vidyasagar, Inorg. Chem 37 (1998) 4764.
[27] B. Vidyavathy, K. Vidyasagar, Inorg. Chem. 38 (1999) 1394.
[28] B. Vidyavathy, K. Vidyasagar, Inorg. Chem. 38 (1999) 3458.
[29] B.N. Gerand, G. Nowogrocki, J. Guenot, M. Figlarz, J. Solid State Chem. 29 (1979) 429.
[30] J.T. Vaughey, W.T.A. Harrison, L.L. Dussack, A.J. Jacobson, Inorg. Chem. 33 (1994) 4370.
[31] W.T.A. Harrison, L.L. Dussack, A.J. Jacobson, Inorg. Chem. 33 (1994) 6043.
[32] W.T.A. Harrison, L.L. Dussack, T. Vogt, A.J. Jacobson, J. Solid State Chem. 120 (1995) 112.
[33] L.L. Dussack, W.T.A. Harrison, A.J. Jacobson, Mater. Res. Bull. 31 (1996) 249.
[34] Z. Otwinowski, Data Collection and Processing, Daresbury Laboratory, Warrington, 1993.
[35] G.M. Sheldrick, SHELXS-97—a program for automatic solution of crystal structures, University of Goettingen, Goettingen, Germany, 1997.
[36] G.M. Sheldrick, SHELXL-97—a program for crystal structure refinement, University of Goettingen, Goettingen, Germany, 1997.
[37] L.J. Farrugia, J. Appl. Cryst. 32 (1999) 837.
[38] M.Y. Chern, R.D. Mariani, D.A. Vennos, F.J. DiSalvo, Rev. Sci. Instrum. 61 (1990) 1733.
[39] S.K. Kurtz, T.T. Perry, J. Appl. Phys. 39 (1968) 3798.
[40] I.D. Brown, D. Altermatt, Acta Crystallogr. B 41 (1985) 244.
[41] N.E. Brese, M. O'Keeffe, Acta Crystallogr. B 47 (1991) 192.
[42] R.D. Shannon, Acta Crystallogr. A 32 (1976) 751.
[43] Y. Dimetriev, J.C.J. Bart, V. Dimitrov, M.Z. Arnaudov, Z. Anorg. Allg. Chem. 479 (1981) 229.
[44] Z. Szaller, L. Kovacs, L. Poppl, J. Solid State Chem. 152 (2000) 392.
[45] M. Arnaudov, V. Dimitrov, Y. Dimitriev, L. Markova, Mater. Res. Bull. 17 (1982) 1121.
[46] J. Laugier, A. Filhol, ERACEL—a program for refinement of the cell parameters, 1978.